

# Nuclear energy density functionals: what we can learn about/from their global performance?

A. V. Afanasjev\*, S. E. Agbemava\*, D. Ray\* and P. Ring†

\**Department of Physics and Astronomy, Mississippi State University, MS 39762, USA*

†*Fakultät für Physik, Technische Universität München, D-85748 Garching, Germany*

**Abstract.** A short review of recent results on the global performance of covariant energy density functionals is presented. It is focused on an analysis of the accuracy of the description of physical observables of ground and excited states as well as to related theoretical uncertainties. In addition, a global analysis of pairing properties is presented and the impact of pairing on the position of two-neutron drip line is discussed.

**Keywords:** Covariant density functional theory, ground states, excited states, theoretical uncertainties

**PACS:** 21.10.Pc, 21.10.Dr, 21.60.Jz, 21.10.Ft

## 1. INTRODUCTION

To fulfill specific requirements of nuclear structure and nuclear astrophysics (such as an high demand for the reliability of theoretical predictions), the *microscopic* and *universal* aspects of nuclear theory should be contemplated. A *microscopic* description by a physically sound model ensures a reliable extrapolation away from the experimentally known region. A *universal* description of all nuclear properties within one unique framework for all nuclei involved ensures a coherent prediction of all unknown data. The quest towards such a theoretical tool will most certainly be in the focus of fundamental nuclear physics research in the foreseeable future. At present, the tool of choice for the description of medium heavy and heavy nuclei is density functional theory (DFT) [1, 2, 3]: for the majority of such nuclei there is simply no other microscopic alternative. Among these nuclear DFT's, covariant density functional theory (CDFT) is one of most attractive since *covariant energy density functionals* (CEDF) exploit basic properties of QCD at low energies, such as symmetries and the separation of scales [2, 4]. They also provide a consistent treatment of the spin degrees of freedom [4], spin-orbit interactions [5, 6] and time-odd mean fields [7, 8].

It is important to understand the accuracy of the description of the properties of the ground and excited states in nuclei, theoretical uncertainties in the description of related physical observables and the predictive power of the models on a global scale. This is especially crucial for nuclear astrophysics, where we are facing the problem of an extrapolation to nuclei with large isospin. Many of such nuclei will not be studied experimentally even with the next generation of facilities, or forever. The advent of high-performance computers has recently allowed to address these questions. As illustrated in Refs. [9, 10], such a global analysis is feasible for ground state observables. On the other hand, for spectroscopic observables such a systematic analysis of the accuracy of the description of experimental data and related theoretical uncertainties has been performed only for actinides [11, 12, 13] because of the complexity of their calculations.

The paper is organized as follows. Some representative examples of the studies of the accuracy of the description of physical observables of ground and excited states and related theoretical uncertainties are presented in Sects. 2 and 3, respectively. Considering that detailed results of these studies have already been published we focus on new results in Sects. 4 and 5. Sect. 4 shows the results of the studies of the global numerical accuracies due to the truncation of the basis in the calculations of binding energies. Sect. 5 presents the results of on-going study of the pairing properties and their impact on the position of two-neutron drip line. Finally, Sect. 6 summarizes the results of our work.

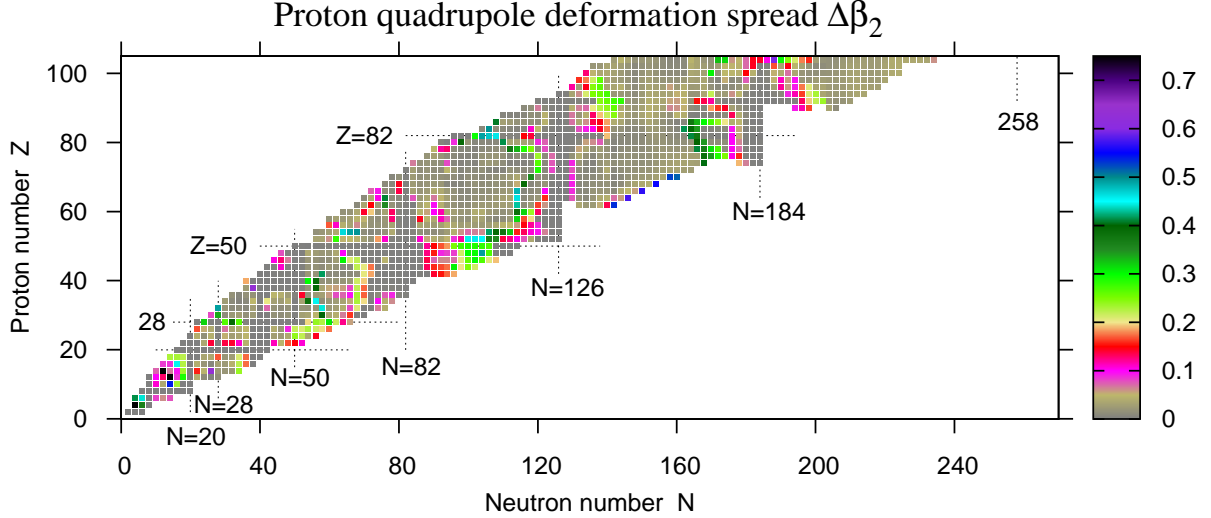


**FIGURE 1.** Proton quadrupole deformation spreads  $\Delta\beta_2(Z,N)$  as a function of proton and neutron number.  $\Delta\beta_2(Z,N) = |\beta_2^{\max}(Z,N) - \beta_2^{\min}(Z,N)|$ , where  $\beta_2^{\max}(Z,N)$  and  $\beta_2^{\min}(Z,N)$  are the largest and smallest proton quadrupole deformations obtained with four employed CEDF's (NL3\*, DD-ME2, DD-ME $\delta$  and DD-PC1) for  $(Z,N)$  nuclei at the ground state.

## 2. GLOBAL PERFORMANCE AND THE ESTIMATE OF THEORETICAL UNCERTAINTIES

The first ever extensive study of global performance of CEDF's has been performed in Refs. [9, 10]. There were two main goals behind this study. First was the assessment of global performance of the state-of-the-art CEDF's with respect of the description of ground state properties of even-even nuclei. The following physical observables were analysed: binding energies, charge radii, neutron skin thicknesses, deformations, the positions of the two-proton and two-neutron drip lines. The analysis of these results will allow in future to define better strategies for new fits of CEDF's. The second goal was to estimate theoretical uncertainties in the description of various physical observables on a global scale and especially in the regions of unknown nuclei.

It was suggested in Refs. [14, 15] to use the methods of information theory and to define the uncertainties in the energy density functional (EDF) parameters. These uncertainties come from the selection of the form of EDF as well as from the fitting protocol details, such as the selection of the nuclei under investigation, the physical observables, or the corresponding weights. Some of them are called *statistical errors* and can be calculated from a statistical analysis during the fit, others are systematic errors, such as for instance the form of the EDF under investigation. On the basis of these statistical errors and under certain assumptions on the independence of the form of many EDF's one hopes to be able to deduce in this way *theoretical error bars* for the prediction of physical observables [14, 15]. The calculation of properties of transitional and deformed nuclei requires a considerable amount of computer time and therefore it is difficult to perform the analysis of statistical errors on a global scale since the properties of all nuclei have to be calculated repeatedly for different variations of original CEDF. Thus, such statistical analysis has been performed mostly for spherical nuclei [14, 16] or selected isotopic chains of deformed nuclei [17].

As a consequence, we concentrate mostly on the uncertainties related to the present choice of EDF's which can be relatively easily deduced globally. We therefore define *theoretical systematic uncertainties* for a given physical observable via the spread of theoretical predictions within the four CEDF's (namely, NL3\* [18], DD-ME $\delta$  [19], DD-ME2 [20] and DD-PC1 [21])

$$\Delta O(Z,N) = |O_{\max}(Z,N) - O_{\min}(Z,N)| \quad (1)$$

where  $O_{\max}(Z,N)$  and  $O_{\min}(Z,N)$  are the largest and smallest values of the physical observable  $O(Z,N)$  obtained with the four employed CEDF's for the  $(Z,N)$  nucleus. Note that these *theoretical uncertainties* are only spreads of physical observables due to a very small number of functionals and, thus, they are only a crude approximation to the *systematic theoretical errors* discussed in Ref. [15].

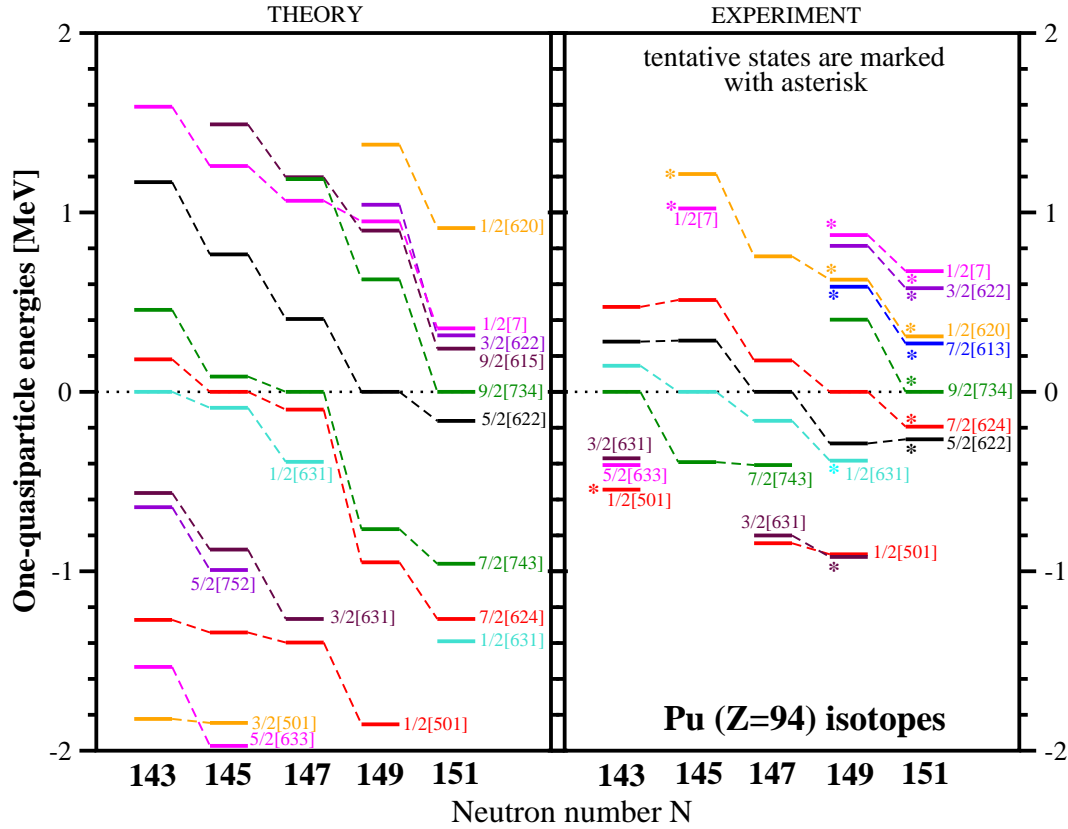


**FIGURE 2.** The evolution of one-quasineutron energies as a function of neutron number for the Pu isotopes. Hole states are plotted below the ground state (zero energy), and particle states are plotted above. Experimental data (one-quasineutron band-head energies) are taken from Ref. [22]. The states are labelled by the Nilsson labels  $\Omega[Nn_z\Lambda]$  or by only principal quantum number  $N$  and  $\Omega$  in the case of strongly mixed wave function.

Although such an analysis has its own merits, at present, it does not allow to estimate real theoretical error bars in the description of physical observables. This is because they originate not only from the uncertainties in model parameters, but also from the definition and the limitations of the model itself. As in the case of present Skyrme functionals, the different CEDF's are far from forming an independent statistical ensemble. Their number is very small and they are all based on a very similar form. For example, no tensor terms are present in the relativistic functionals under investigation and simple power laws are used for the density dependence in the Skyrme DFT. The parameters of these functionals are fitted according to similar protocols including similar types of physical observables such as binding energies and radii. In addition, there exist principal theoretical deficiencies for all presently used nuclear density functionals. Although there exist formal mathematical existence theorems for exact density functionals in an external field [23], a similar theorem has not been proven for self-bound systems such as nuclei [24, 25, 26]. In addition, there is the problem of shape coexistence in transitional nuclei, where the superposition of nuclei with different shapes has to be described by a linear combination of Slater determinants, i.e. by the methods going beyond mean field, and, therefore, beyond the concept of conventional density functional theory [27]. The later uncertainties are very difficult to estimate. As a consequence, any analysis of theoretical uncertainties (especially, for extrapolations to neutron-rich nuclei) contains a degree of arbitrariness related to the choice of the model and fitting protocol in detail and to the concept of density functional theory in nuclei in general.

Fig. 1 shows an example of such analysis of theoretical uncertainties; in this case ground state proton quadrupole deformations are considered. Theoretical uncertainties for this physical observable are either non-existent or very small for spherical or nearly spherical nuclei as well as for well-deformed nuclei in the rare-earth and in the actinide regions. The largest spreads for predicting the equilibrium quadrupole deformations exist at the boundaries between regions of different deformations. They are extremely high in the regions of the prolate-oblate shape coexistence, indicating that the ground state in a given nucleus can be prolate (oblate) in one CEDF and oblate (prolate) in another CEDF. These

uncertainties are due to the deficiencies of the current generations of the DFT models with respect of the description of single-particle energies [10].

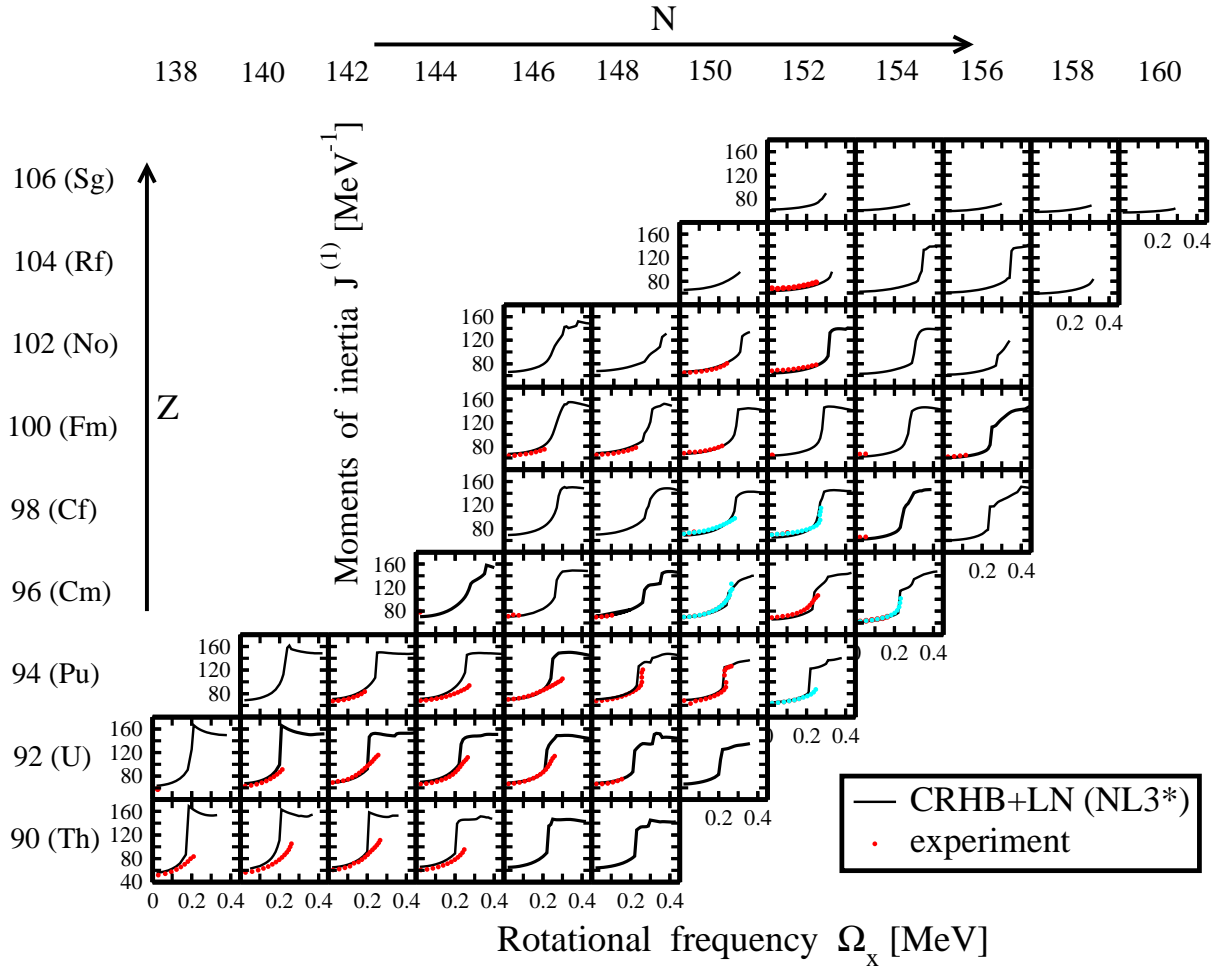


**FIGURE 3.** Experimental and calculated moments of inertia  $J^{(1)}$  as a function of rotational frequency  $\Omega_x$ . The calculations are performed with the NL3\* CEDF [18]. Calculated results and experimental data are shown by black lines and red dots, respectively. Cyan dots are used for new data (Ref. [28]) which became available after publication of Ref. [12]. From Ref. [13].

### 3. SYSTEMATIC STUDIES IN SPECIFIC REGIONS OF NUCLEAR CHART

As illustrated in Fig. 1, the theoretical uncertainties in the prediction of ground state proton quadrupole deformations are rather small for the regions of well deformed nuclei such as rare-earth and actinides. Moreover, the experimental data on  $\beta_2$  in these regions are well (typically within the experimental uncertainties) described by CDFT (see Sect. IX in Ref. [10]). As a result, such experimental data cannot be used to differentiate between the functionals. It turns out that the biggest difference between the CEDF's exists for the single-particle spectra (see, for example, Ref. [29]).

Fig. 2 shows an example of the comparison between calculated and experimental one-quasineutron spectra in Pu isotopes [11]. This reference represent most comprehensive study (among any DFT) of the single-particle excitations in deformed systems. A number of features are clearly seen. First, for a given 1-qp state the discrepancy between theory and experiment depends on neutron number. Second, for a given 1-qp state the slope of the energy curve as a function of neutron number is more pronounced in the calculations than in experiment. These two features are interconnected and they emerge from the fact that theoretical energy scale is more stretched out than the experimental one due to the low effective mass. The change of the Fermi energy with neutron number leads to changes of the energy differences between ground and excited states and these differences are affected by the effective mass in the calculations. Third,

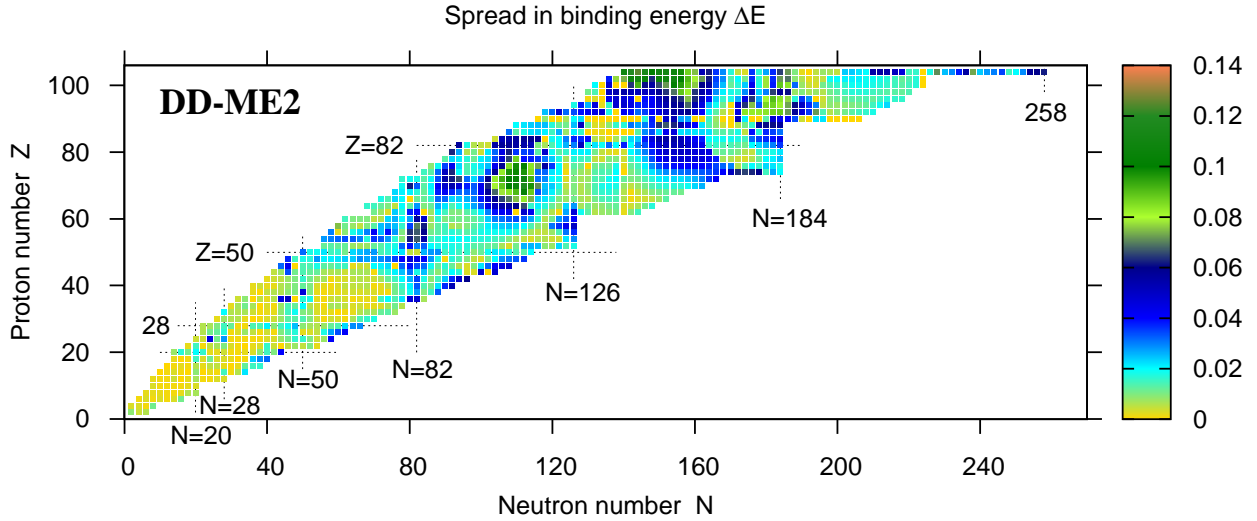


**FIGURE 4.** The spread of calculated binding energies when different deformations of the basis are used in the calculations. See text for details.

the relative energies of different experimental 1-qp states are not always reproduced in the calculations. This feature originates from the fact that the energies of spherical subshells, from which the deformed states emerge, can deviate from experiment [29]). These three features are seen in all isotone and isotope chains.

It is also interesting to see how other spectroscopic observables are described in experiment and how they depend on the choice of the CEDF. Fig. 3 shows the results of the first ever (in any DFT framework) systematic investigation of rotational properties of even-even nuclei at normal deformation [12]. The calculations are performed within the cranked relativistic Hartree-Bogoliubov (CRHB) approach with approximate particle number projection by means of the Lipkin-Nogami method (further CRHB+LN) [30]. One can see that the moments of inertia below band crossings are reproduced well. The upbendings observed in a number of rotational bands of the  $A \geq 242$  nuclei are also reasonably well described in the model calculations. Moreover, the CRHB+LN approach has a good predictive power as illustrated by the fact that new data (cyan dots) are very close to model predictions. However, the calculations also predict similar upbendings in lighter nuclei, but they have not been seen in experiment. The analysis suggests that the stabilization of octupole deformation at high spin, not included in the present CRHB+LN calculations, could be responsible for this discrepancy between theory and experiment [12]. With few exceptions, the rotational properties of one-quasiparticle configurations, which yield important information on their underlying structure and, thus, provide an extra tool for configuration assignment, are also well described in the CRHB+LN calculations (see Ref. [12] for details).

#### 4. THE ESTIMATE OF NUMERICAL UNCERTAINTIES IN THE CALCULATIONS OF BINDING ENERGIES

In the RHB calculations of Ref. [10], the truncation of the basis is performed in such a way that all states belonging to the major shells up to  $N_F = 20$  fermionic shells for the Dirac spinors and up to  $N_B = 20$  bosonic shells for the meson fields are taken into account. Note that a similar truncation of the basis is usually used in the fitting protocols of the state-of-the-art CEDF's. For each nucleus the potential energy curve is calculated in a large deformation range from  $\beta_2 = -0.4$  up to  $\beta_2 = 1.0$  by means of the constraint on the quadrupole moment  $q_{20}$ . In constrained calculations, the deformation of the basis is selected in such a way that it corresponds to the desired deformation of the converged solution. The lowest in energy minimum is defined from the potential energy curve. Then, unconstrained calculations are performed in this minimum and the correct ground state configuration and its energy are determined. This procedure is especially important for the cases of shape coexistence.

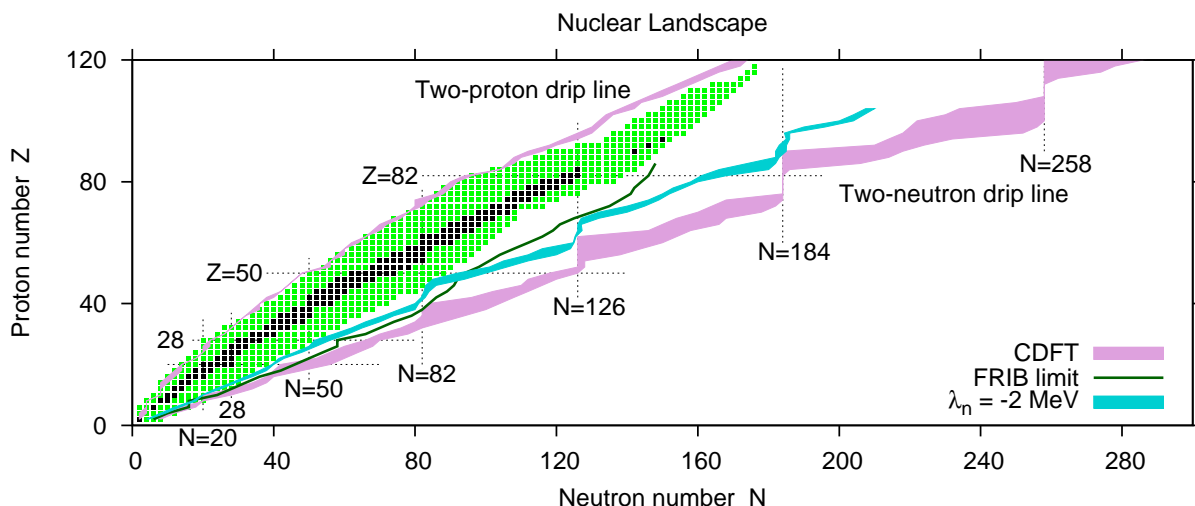


**FIGURE 5.** Nuclear landscape as provided by state-of-the-art CDFT calculations. The uncertainties in the definition of two-proton and two-neutron drip lines are shown by violet shaded areas. They are defined by the extremes of the predictions of the corresponding drip lines obtained with different functionals. The uncertainties (the range of nuclei) in the definition of the neutron chemical potential  $\lambda_n = -2.0$  MeV are shown by blue shaded area. Experimentally known stable and radioactive (including proton emitters) nuclei are shown by black and green squares, respectively. Green solid line shows the limits of the nuclear chart (defined as fission yield greater than  $10^{-6}$ ) which may be achieved with dedicated existence measurements at FRIB [31]. Based on Fig. 4 of Ref. [9].

It is important to estimate how the selection of the basis affects the calculated binding energies in the unconstrained calculations. In order to address this question the calculations for all even-even nuclei under study have been performed with the DD-ME2 CEDF employing eight values of the deformation of the basis starting from  $\beta_2 = -0.3$  and increasing up to  $\beta_2 = 0.4$  in step of 0.1. Then in each nucleus the spread of calculated binding energies has been calculated as a difference of the minimal and maximal binding energies obtained in the ground state minimum. These spreads are shown in Fig. 4. One can see that they are below 20 keV in the absolute majority of light nuclei. These spreads are higher in medium and heavy mass nuclei. However, even there they are below 100 keV.

Unconstrained calculations for a given deformation of basis do not always converge to the ground state minimum. This typically takes place in transitional nuclei with soft potential energy surfaces and nuclei with prolate-oblate shape coexistence. In these nuclei, the calculated binding energies of only a few deformations of the basis enter in the definition of the spreads. As a result, these spreads are smaller than in well-deformed nuclei. On the other hand, in well-deformed nuclei almost all employed deformations of the basis lead to the ground state minimum in the calculations. That is a reason why among  $Z \geq 50$  nuclei the spreads of binding energies are most pronounced in the well-deformed nuclei of the rare-earth region and the actinides (Fig. 4).

This analysis clearly shows that the employed truncation of basis provides accurate results; extremely small numerical errors exist in light nuclei but they increase somewhat with the increase of the mass of the nucleus. Note that the same approach has been used in unconstrained calculations of Ref. [10]; the binding energy of the ground state configuration has been defined as a minimum energy of the unconstrained calculations obtained for eight deformations of the basis. It was also observed that not always the lowest in energy solution is generated by the deformation of the basis which is close to the deformation of the solution.

## 5. PAIRING PROPERTIES

Other interesting questions are the evolution of pairing properties with isospin, their dependence on the CEDF's, the uncertainties in their definition and the impact of these factors on the physical observables of interest. There are two measures of pairing correlations, namely, the pairing gap  $\Delta$  and the pairing energies  $E_{pairing}$ . In addition, the energies of proton or neutron chemical potentials and their evolution with particle number are important for the definition of the positions of the proton and neutron drip lines and the regions of the nuclear chart where the coupling with the

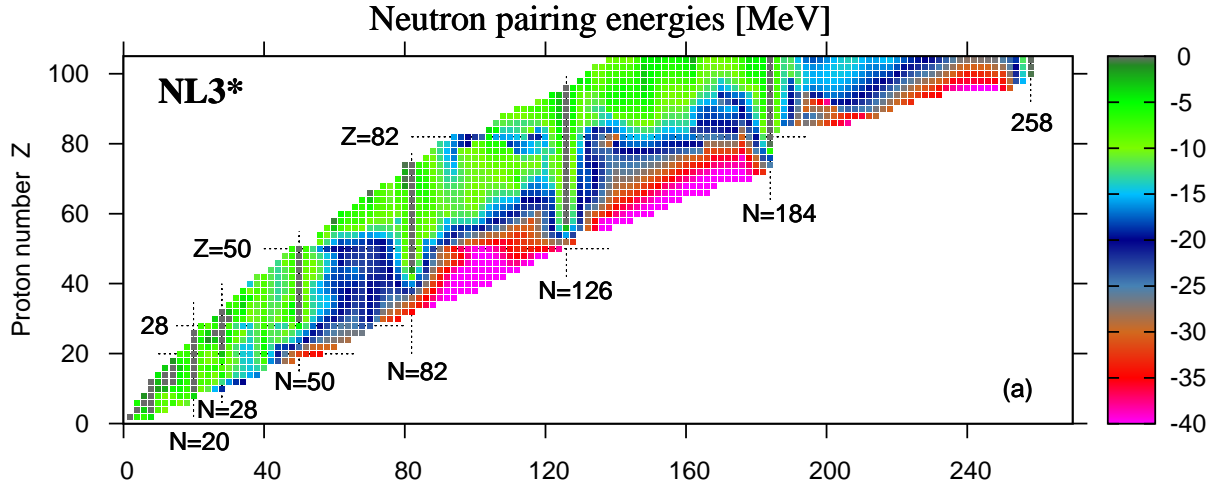


FIGURE 6. Neutron pairing energies  $E_{pairing}$  obtained in the RHB calculations with the NL3\* CEDF.

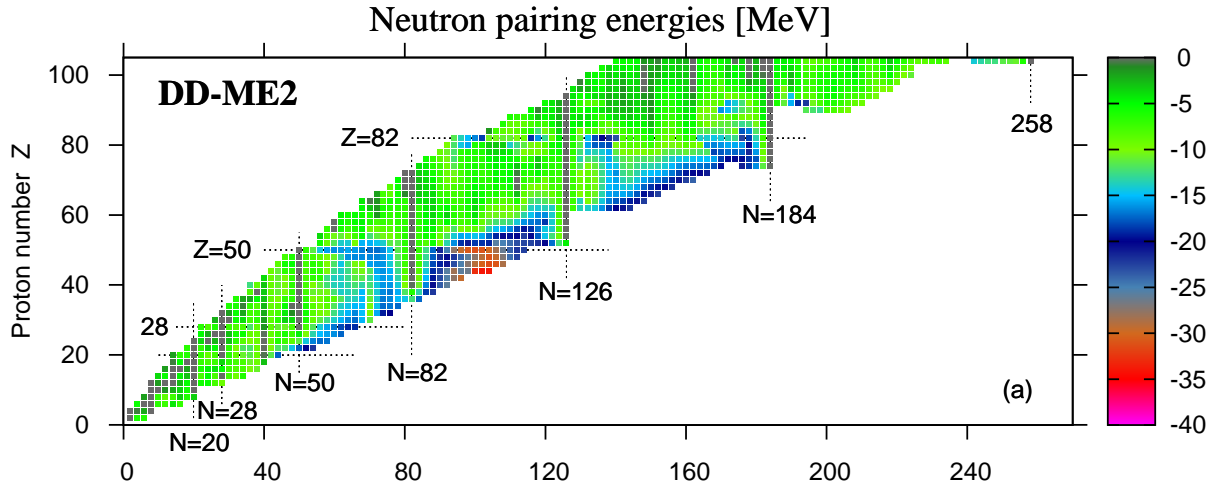
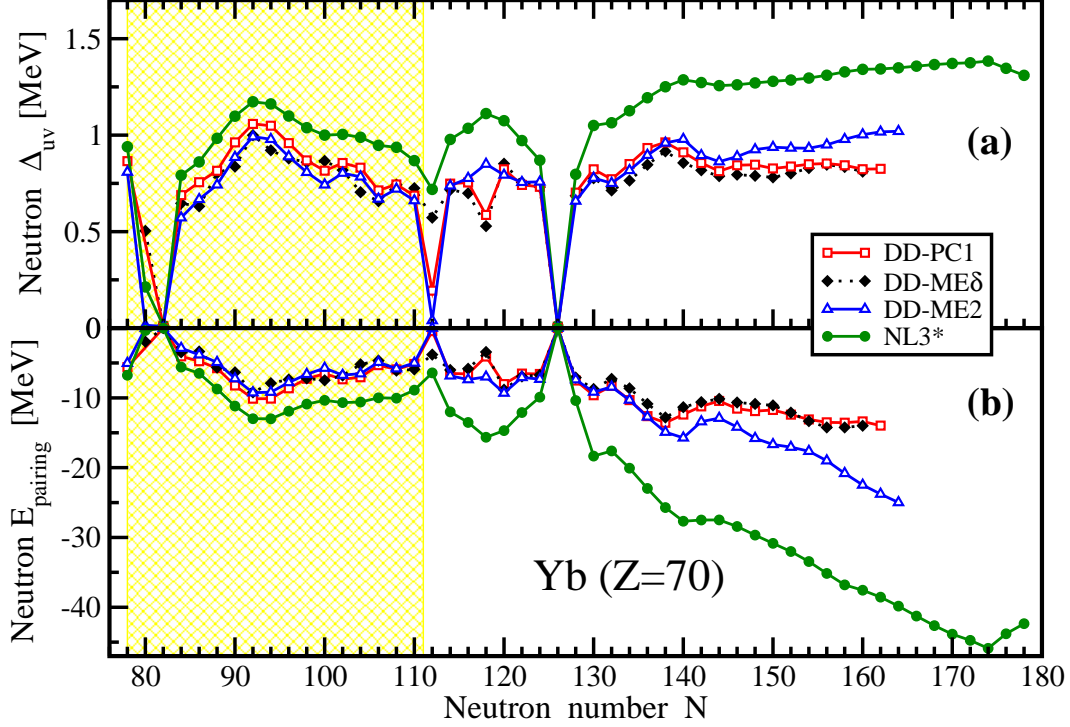


FIGURE 7. The same as Fig. 6 but for the DD-ME2 CEDF.

continuum may become important. Fig. 5 shows the nuclear landscape as obtained with four state-of-the-art CEDF's (NL3\*, DD-ME2, DD-PC1 and DD-ME $\delta$ ) and related theoretical uncertainties in the definition of the two-proton and two-neutron drip lines [9]. In addition, this figure compares the uncertainties (the range of nuclei) in the definition of the neutron chemical potential  $\lambda_n = -2.0$  MeV (blue shaded area) with a possible extension (green solid line) of the nuclear landscape by means of the facility for the rare isotope beams (FRIB). These 2 MeV represents roughly the typical size of the energy window above and below the chemical potential in which the pairing interaction affects measurably the occupation of the single-particle orbitals. If the neutron chemical potential of a given nucleus is closer than 2 MeV to the continuum, the pairing interaction can scatter pairs to the continuum. Thus, Fig. 5 suggests that in future FRIB experiments the region of nuclei with measurable coupling with the continuum can be reached only in



**FIGURE 8.** Neutron pairing gaps  $\Delta_{uv}$  and pairing energies  $E_{pairing}$  of the Yb nuclei located between the two-proton and two-neutron drip-lines obtained in the axial RHB calculations with the indicated CEDF's. The shaded yellow area indicates experimentally known nuclei.

the  $Z \leq 50$  nuclei. For higher  $Z$  nuclei, future experimental data on neutron-rich nuclei can be safely treated without accounting of the coupling with the continuum.

At present, several definitions of the pairing gap exist [10]. However, the analysis presented in Sect. IV of Ref. [10] clearly indicates that the  $\Delta_{uv}$  values for the pairing gap defined in even-even nuclei provide the best agreement with the pairing indicators calculated from odd-even mass staggerings. The pairing gap

$$\Delta_{uv} = \frac{\sum_k u_k v_k \Delta_k}{\sum_k u_k v_k} \quad (2)$$

averages over  $u_k v_k$ , a quantity which is concentrated around the Fermi surface. In Hartree-(Fock)-Bogoliubov calculations the size of the pairing correlations is usually measured in terms of the pairing energy defined as

$$E_{pairing} = -\frac{1}{2} \text{Tr}(\Delta \kappa). \quad (3)$$

This is not an experimentally accessible quantity, but it is a measure for the size of the pairing correlations in theoretical calculations.

Figs. 6 and 7 compare neutron pairing energies  $E_{pairing}$  obtained with the NL3\* and DD-ME2 CEDF's. In the region of known nuclei these energies are only slightly smaller (but, in general, quite comparable) in DD-ME2 as compared with NL3\*. However, on approaching the two-neutron drip line, substantial differences develop between the pairing energies in the RHB calculations with these two CEDF's. The absolute values of neutron pairing energies obtained in RHB calculations with NL3\* are by factor of 3-4 higher near the two-neutron drip line than those in known the nuclei (Fig. 6). This difference reduces to a factor 2 for the DD-ME2 CEDF (Fig. 7). The results obtained with DD-MEδ and DD-PC1 are similar to the ones obtained with DD-ME2.

Unfortunately, at present similar figures cannot be generated for the  $\Delta_{uv}$  pairing gaps because of an improper recording of this quantity during the production calculations for Ref. [10]. Thus, we perform the comparison of the evolution of neutron pairing gaps  $\Delta_{uv}$  and pairing energies  $E_{pairing}$  as a function of neutron number only for the Yb



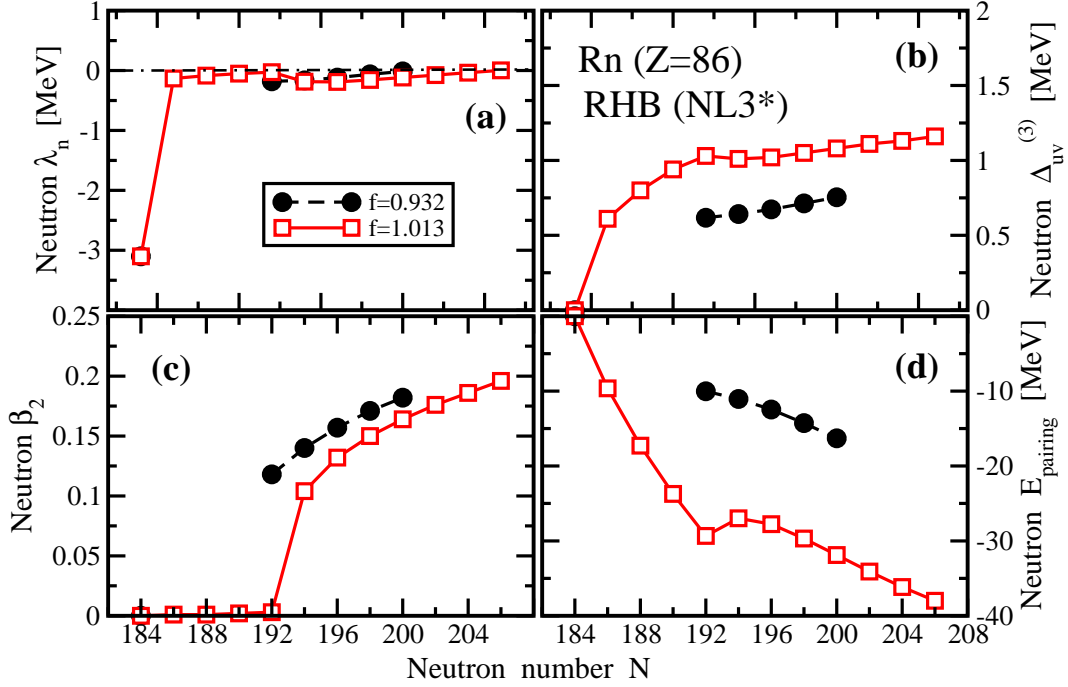


**FIGURE 9.** The evolution of neutron chemical potential  $\lambda_n$  (panel (a)), neutron quadrupole deformation  $\beta_2$  (panel (c)), neutron pairing gap  $\Delta_{uv}$  (panel (b)) and neutron pairing energy  $E_{pairing}$  (panel (d)) as a function of neutron number  $N$  in the Rn isotopes with  $N \geq 184$  obtained in the RHB (NL3\*) calculations. Only the results for bound nuclei are shown. The results of the calculations for two values of scaling factor  $f$  of separable pairing force of finite range are presented. Note that the value of  $f = 1.013$  has been used in the calculations of Ref. [10].

$Z = 70$  isotope chain (see Fig. 8). One can see that in the RHB calculations with the DD-ME $\delta$ , DD-ME2 and DD-PC1 CEDF's the pairing gaps  $\Delta_{uv}$  in neutron-rich  $N \geq 126$  nuclei have on average the same magnitude as pairing gaps in known nuclei (Fig. 8a). However, the absolute pairing energies are larger by a factor of about 2 in neutron-rich nuclei as compared with the ones in known nuclei. Note that both  $\Delta_{uv}$  and  $E_{pairing}$  are more or less constant in neutron-rich nuclei in the RHB calculations with DD-PC1 and DD-ME $\delta$ . On the contrary, some increase of absolute values of these quantities with increasing isospin is observed in DD-ME2.

The situation is different in the NL3\* CEDF. The pairing is somewhat stronger in known nuclei as compared with DD CEDF's. However, more pronounced differences are seen when the results in neutron-rich nuclei are compared with the ones in known nuclei. The pairing gaps  $\Delta_{uv}$  are on average 25% larger in neutron-rich nuclei as compared with known ones and, in addition, they gradually increase with neutron number. The absolute values of the pairing energies rapidly increase with neutron number in neutron-rich  $N \geq 126$  nuclei; near two-proton drip line these energies are larger by a factor of 4 than average pairing energies in known nuclei.

Note that in Ref. [10], the selection of scaling factors  $f$  for separable pairing has been guided by the comparison of experimental data with different calculations based on the NL3\* CEDF. The same scaling factors  $f$  were used also in the calculations with DD-PC1, DD-ME2 and DD-ME $\delta$ . The spread in the calculated values  $\Delta_{uv}$  values in known nuclei indicates that the scaling factors  $f$  used in Ref. [10] are reasonable within few % (see Sec. IV in Ref. [10] and Fig. 8 in the present paper). The weak dependence of the scaling factor  $f$  on the CEDF has already been seen in the studies of pairing and rotational properties in the actinides [29, 12]. Considering the global character of the study in Ref. [10], this is a reasonable choice. Definitely there are nuclei in which the choice of the scaling factors  $f$  is not optimal.

Considering the differences in the predictions of the pairing properties of the nuclei near the drip line, it is important to understand how they affect physical observables of interest such as the position of two-neutron drip line. To address this question we analyze the chain of Rn ( $Z = 86$ ) isotopes, the two-neutron drip lines of which are located at  $N = 206$  for NL3\* and at  $N = 184$  for DD-ME2, DD-ME $\delta$ , and DD-PC1 in the calculations of Ref. [10].

First, we perform the RHB(NL3\*) calculations with a pairing strength decreased by 8% (scaling factor  $f = 0.932$ )

as compared to the one used in Ref. [10]. This will roughly put the calculated pairing energies near the two-proton drip line into the range close to the one obtained in the calculations with DD-ME $\delta$ , DD-ME2 and DD-PC1 CEDF's (compare Figs. 7 and 9d). This decrease of pairing strength has a significant effect on the nuclei near the two-neutron drip line and the position of the two-neutron drip line. Indeed, the Rn isotopes with  $N = 186, 188, 190, 202, 204$  and  $206$ , which are bound for the original strength of pairing (scaling factor  $f = 1.013$ ), become unbound for decreased pairing. In addition, the deformations of the  $N = 192 - 200$  isotopes become larger (Figs. 9c); this reflects the well known fact that pairing typically tries to make a nucleus less deformed.

Second, we try to bring the situation in the RHB calculations with the DD CEDF's close to the one seen in NL3\* by increasing the pairing strength by 8% in the RHB calculations with DD-ME2 and DD-PC1. However, this does not affect the position of two-neutron drip lines for the Rn isotope chain in these CEDF's because of the details of the underlying shell structure. These two results clearly show that the actual position of the two-neutron drip line sensitively depends on fine details of the underlying shell structure and the strength of pairing.

## 6. CONCLUSIONS

During the last several years considerable progress in an understanding of the global performance of state-of-the-art covariant energy density functionals and related theoretical uncertainties has been achieved. Many physical observables related to the ground state properties (binding energies, charge radii, deformations, neutron skin thicknesses, the positions of drip lines etc), the properties of excited states (moments of inertia, energies of predominantly single-particle states, fission barriers [32] etc) have been studied either globally or at least systematically in a specific region of nuclear chart. Theoretical uncertainties for many physical observables have been defined. The current generation of CEDF's has been fitted only to bulk and nuclear matter properties. The existing discrepancies between theory and experiment clearly indicate the need for the inclusion of single-particle information into the fitting protocol of next generation of CEDF's. It is doubtful that without inclusion of such information missing terms (and missing physics) of CEDF's can be identified.

## ACKNOWLEDGMENTS

This work has been supported by the U.S. Department of Energy under the grant DE-FG02-07ER41459 and by the DFG cluster of excellence "Origin and Structure of the Universe" (www.universe-cluster.de). This work was also partially supported by an allocation of advanced computing resources provided by the National Science Foundation. The computations were partially performed on Kraken at the National Institute for Computational Sciences (<http://www.nics.tennessee.edu/>).

## REFERENCES

1. W. Kohn, *Rev. Mod. Phys.* **71**, 1253–1266 (1999).
2. *Extended Density Functionals in Nuclear Structure Physics*, Lecture Notes in Physics, edited by G. A. Lalazissis, P. Ring, and D. Vretenar (Springer-Verlag, Heidelberg, 2004) **Vol. 641** (2004).
3. J. E. Drut, R. J. Furnstahl, and L. Platter, *Prog. Part. Nucl. Phys.* **64**, 120 (2010).
4. D. Vretenar, A. V. Afanasjev, G. A. Lalazissis, and P. Ring, *Phys. Rep.* **409**, 101 (2005).
5. M. Bender, K. Rutz, P.-G. Reinhard, J. A. Maruhn, and W. Greiner, *Phys. Rev. C* **60**, 034304 (1999).
6. E. V. Litvinova, and A. V. Afanasjev, *Phys. Rev. C* **84**, 014305 (2011).
7. J. König, and P. Ring, *Phys. Rev. Lett.* **71**, 3079 (1993).
8. A. V. Afanasjev, and H. Abusara, *Phys. Rev. C* **81**, 014309 (2010).
9. A. V. Afanasjev, S. E. Agbemava, D. Ray, and P. Ring, *Phys. Lett. B* **726**, 680 (2013).
10. S. E. Agbemava, A. V. Afanasjev, D. Ray, and P. Ring, *Phys. Rev. C* **89**, 054320 (2014).
11. A. V. Afanasjev, and S. Shawaqfeh, *Phys. Lett. B* **706**, 177 (2011).
12. A. V. Afanasjev, and O. Abdurazakov, *Phys. Rev. C* **88**, 014320 (2013).
13. A. V. Afanasjev, *Phys. Scr.* **89**, 054001 (2014).
14. P. G. Reinhard, and W. Nazarewicz, *Phys. Rev. C* **81**, 051303(R) (2010).
15. J. Dobaczewski, W. Nazarewicz, and P.-G. Reinhard, *J. Phys. G* **41**, 074001 (2014).
16. M. Kortelainen, J. Erler, W. Nazarewicz, N. Birge, Y. Gao, and E. Olsen, *Phys. Rev. C* **88**, 031305(R) (2013).
17. J. Erler, N. Birge, M. Kortelainen, W. Nazarewicz, E. Olsen, A. M. Perhac, and M. Stoitsov, *Nature* **486**, 509 (2012).

18. G. A. Lalazissis, S. Karatzikos, R. Fossion, D. P. Arteaga, A. V. Afanasjev, and P. Ring, *Phys. Lett.* **B671**, 36 (2009).
19. X. Roca-Maza, X. Viñas, M. Centelles, P. Ring, and P. Schuck, *Phys. Rev. C* **84**, 054309 (2011).
20. G. A. Lalazissis, T. Nikšić, D. Vretenar, and P. Ring, *Phys. Rev. C* **71**, 024312 (2005).
21. T. Nikšić, D. Vretenar, and P. Ring, *Phys. Rev. C* **78**, 034318 (2008).
22. *Evaluated Nuclear Structure Data File (ENSDF) located at the website (<http://www.nndc.bnl.gov/ensdf/>) of Brookhaven National Laboratory. ENSDF is based on the publications presented in Nuclear Data Sheets (NDS) which is a standard for evaluated nuclear data. Adopted experimental one-quasiparticle levels are taken from the NDS articles published during 2001-2011.* (2012).
23. P. Hohenberg, and W. Kohn, *Phys. Rev.* **136**, B864 (1964).
24. J. Engel, *Phys. Rev. C* **75**, 014306 (2007).
25. B. G. Giraud, *Phys. Rev. C* **77**, 014311 (2008).
26. T. Nakatsukasa, *Prog. Theor. Exp. Phys.* **01A207** (2012).
27. T. Nikšić, D. Vretenar, and P. Ring, *Prog. Part. Nucl. Phys.* **66**, 519 (2011).
28. S. Hota, *PhD thesis, University of Massachusetts, Lowell* (2012).
29. A. V. Afanasjev, T. L. Khoo, S. Frauendorf, G. A. Lalazissis, and I. Ahmad, *Phys. Rev. C* **67**, 024309 (2003).
30. A. V. Afanasjev, P. Ring, and J. König, *Nucl. Phys.* **A676**, 196 (2000).
31. H. Schatz, *private communication, see also <https://groups.nsl.msu.edu/frib/rates/fribrates.html>* (2014).
32. H. Abusara, A. V. Afanasjev, and P. Ring, *Phys. Rev. C* **82**, 044303 (2010).